

Kinetic isotope effects of $^{12}\text{CH}_3\text{D} + \text{OH}$ and $^{13}\text{CH}_3\text{D} + \text{OH}$ from 278 to 313 K

L. M. T. Joelsson^{1,3}, J. A. Schmidt¹, E. J. K. Nilsson², T. Blunier³, D. W. T. Griffith⁴, S. Ono⁵, and M. S. Johnson¹

¹Department of Chemistry, University of Copenhagen, Copenhagen, Denmark

²Division of Combustion Physics, Department of Physics, Lund University, Sweden

³Centre for Ice and Climate (CIC), Niels Bohr Institute, University of Copenhagen, Copenhagen, Denmark

⁴University of Wollongong, Department of Chemistry, Wollongong, Australia

⁵Department of Earth, Atmospheric and Planetary Sciences, Massachusetts Institute of Technology, Cambridge, MA, USA

Correspondence to: M. S. Johnson (msj@kiku.dk)

Abstract. Methane is the second most important long lived greenhouse gas and plays a central role in the chemistry of the Earth's atmosphere. Nonetheless there are significant uncertainties in its source budget. Analysis of the isotopic composition of atmospheric methane, including the doubly substituted species $^{13}\text{CH}_3\text{D}$ offers new insight on the methane budget as the sources and sinks have distinct isotopic signatures. The most important sink of atmospheric methane is oxidation by OH in the troposphere which accounts for around 84% of all methane removal. Here we present experimentally derived methane + OH kinetic isotope effects and their temperature dependence over the range of 278 to 313 K for CH_3D and $^{13}\text{CH}_3\text{D}$; the latter is reported here for the first time. We find $k_{\text{CH}_4}/k_{\text{CH}_3\text{D}} = 1.31 \pm 0.01$ and $k_{\text{CH}_4}/k_{^{13}\text{CH}_3\text{D}} = 1.34 \pm 0.03$ at room temperature, implying that the methane + OH kinetic isotope effect is multiplicative such that $(k_{\text{CH}_4}/k_{^{13}\text{CH}_4})(k_{\text{CH}_4}/k_{\text{CH}_3\text{D}}) = k_{\text{CH}_4}/k_{^{13}\text{CH}_3\text{D}}$, within the experimental uncertainty, given the literature value of $k_{\text{CH}_4}/k_{^{13}\text{CH}_4} = 1.0039 \pm 0.0002$. In addition, the kinetic isotope effects were characterized using transition state theory with tunneling corrections. Good agreement between the experimental, quantum chemical, and available literature values was obtained. The theoretical calculation confirms that the $^{13}\text{CH}_3\text{D}$ isotope effect is the product of D- and ^{13}C - isotope effects. Based on the results we conclude that the OH reaction (the main sink of methane) at steady-state can produce an atmospheric clumped isotope signal ($\Delta(^{13}\text{CH}_3\text{D}) = \ln([\text{CH}_4][^{13}\text{CH}_3\text{D}]/[^{13}\text{CH}_4][\text{CH}_3\text{D}])$) of 0.02 ± 0.02 . This implies that the bulk tropospheric $\Delta(^{13}\text{CH}_3\text{D})$ reflects the source signal with relatively small adjustment due to the sink signal (i.e. mainly OH oxidation).

20 1 Introduction

Atmospheric methane is the subject of increasing interest from both the climate research community and the public due its impacts on climate change, as reported by the IPCC (2013). The direct radiative forcing of methane is 0.64 Wm^{-2} . Including feedback mechanisms and secondary effects e.g. increased O_3 production, stratospheric water vapor and production of CO_2 , methane's radiative forcing becomes 0.97 Wm^{-2} , 2/3 of the forcing by CO_2 over the same time period (IPCC, 2013, Fig. 8.15).

Atmospheric methane has both natural and anthropogenic sources and the two categories contribute about equally (Ciais et al., 2013, and references therein). Wetlands are the dominant natural source, and agriculture and waste are the largest anthropogenic sources. Fossil fuels make smaller contributions. A majority (84%) of atmospheric methane is removed by oxidation by OH in the troposphere:



while oxidation in the troposphere by Cl contributes about 4% of the total:



35 About 8% of methane is removed in the stratosphere by radical oxidation, such as reactions (R2) and (R3):



The rest (4%) is removed by soil (Kirschke et al., 2013).

Carbon and hydrogen isotopic analysis are widely used to distinguish microbial and thermal sources of atmospheric methane (e.g., Lowe et al., 1997; Ferretti et al., 2005; Tyler et al., 2007; Lassey et al., 2007). However, reactions (R1), (R2), and (R3) produce relatively large D/H isotope effects (Saueressig et al., 1995, 1996, 2001; Crowley et al., 1999; Feilberg et al., 2005). Thus, the construction of an accurate top-down methane budget by isotopic analysis must take the isotopic signatures of both sources and sinks into account (Quay et al., 1999; Bergamaschi et al., 2000; Allan et al., 2001a, b). An isotope budget based on methane source (and sink) fractionations is an underdetermined systems (e.g., Pohlman et al., 2009). Recent advances in mass spectrometry (Eiler et al., 2013; Stolper et al., 2014) and laser infrared spectroscopy (Ono et al., 2014; Wang et al., 2015) facilitate measurement of rare double-substituted isotopologues. The abundance of these "clumped" isotopologues (clumped refers to the rare isotopes being clumped together) generally follows a stochastic distribution (i.e. $[{}^{12}\text{CH}_4][{}^{13}\text{CH}_3\text{D}] = [{}^{13}\text{CH}_4][{}^{12}\text{CH}_3\text{D}]$). However, small deviations from stochastic distribution can be induced by thermodynamic (Ma et al., 2008; Stolper et al., 2014; Liu and Liu, 2016), kinetic (Joelsson et al., 2014; Wang et al., 2015), and photolytic processes (Schmidt et al., 2013; Schmidt and Johnson, 2015). Analysis of the clumped isotope anomaly in methane will yield

unique constraints for the methane budget. Optical methods, as will be shown in this paper, provide
 55 high throughput and accuracy for overcoming the problems of analysis of clumped CH₄. The dif-
 ference and advantage of this approach is the additional information not available in single isotope
 analysis, especially regarding the mechanism of formation, independent of the enrichment of D and
¹³C in the starting material.

The kinetic isotope effect ^jE_α is a characteristic property of each process:

$$60 \quad {}^j\text{E}_\alpha \equiv \frac{k({}^i\text{E} + \text{OH})}{k({}^j\text{E} + \text{OH})}, \quad (1)$$

where ⁱE is the most abundant (here, the lighter) isotopologue, ^jE the rare (heavy) isotopologue,
 k(E + OH) is the reaction rate coefficient for the reaction E + OH. As a measure of how much
 of a fractionation of ¹³CH₃D kinetic reactions produce, the apparent clumpiness, γ is used. It is a
 measure of the effect of the clumped substitution on the reaction rate, as opposed to the combined
 65 effect of two single substitutions. It is defined as (Wang et al., 2015):

$$\gamma \equiv \frac{{}^{13}\text{C,D}_\alpha}{{}^{13}\text{C}_\alpha \times \text{D}_\alpha} \quad (2)$$

A related measure is the Δ(¹³CH₃D) value that quantifies the extent to which rare isotopes clump
 together to form a multiply substituted species, as opposed to a stochastic distribution (Ono et al.,
 2014):

$$70 \quad \Delta({}^{13}\text{CH}_3\text{D}) \equiv \ln \left(\frac{[{}^{13}\text{CH}_3\text{D}][{}^{12}\text{CH}_4]}{[{}^{12}\text{CH}_3\text{D}][{}^{13}\text{CH}_4]} \right), \quad (3)$$

where [¹³CH₃D], [¹²CH₄], [¹²CH₃D] and [¹³CH₄] represent the concentrations of the different iso-
 topologues.

The kinetic isotope effects for the singly substituted species CH₃D and ¹³CH₄ have been studied
 previously both experimentally and theoretically, see Tables 3 and 4 respectively. The kinetic isotope
 75 effect ¹³C,D_α for the reaction with OH is not described in the existing literature. The related kinetic
 isotope effect for the CH₄ + Cl reaction was measured at room temperature with the present setup
 by Joelsson et al. (2014) and found to be 1.60 ± 0.04. The kinetic isotope effects in the doubly
 substituted methane isotopologue CH₂D₂ for the reaction CH₄ + Cl has been studied previously by
 Feilberg et al. (2005).

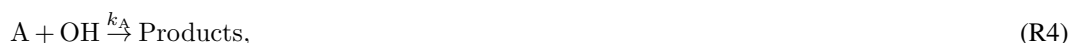
80 In the present study the kinetic isotope effects ^Dα and ¹³C,D_α are determined using the relative rate
 method. Species concentrations in the reaction cell are determined using Fourier Transform Infrared
 (FTIR) spectroscopy. Further, ^Dα, ¹³C_α, and ¹³C,D_α are calculated using quantum chemistry and
 transition state theory.

2 Experimental procedures

85 16 experiments were conducted, numbered from 1 through 16, see Table 1; eight (Experiments 1–8) for $^{12}\text{CH}_3\text{D}$ and eight (Experiments 9–16) for $^{13}\text{CH}_3\text{D}$. The experiments were conducted at four different temperatures ($T = 278, 288, 298, 313\text{K} = 5, 15, 25, 40^\circ\text{C}$); two experiments were conducted for each temperature.

2.1 Relative rate method

90 The experiments were carried out using the relative rate method on a semi-static gas mixture. The decaying concentrations of reactants were measured as a function of the extent of reaction. Considering two bimolecular reactions with second order rate coefficients k_A and k_B ,



95 and assuming there were no other loss processes, the following relation holds:

$$\ln\left(\frac{[\text{A}]_0}{[\text{A}]_t}\right) = \frac{k_A}{k_B} \ln\left(\frac{[\text{B}]_0}{[\text{B}]_t}\right). \quad (4)$$

Here $[\text{A}]_0$, $[\text{A}]_t$, $[\text{B}]_0$ and $[\text{B}]_t$ represent the concentrations of compounds A and B at times 0 and t respectively. The slope of $\ln([\text{A}]_0/[\text{A}]_t)$ versus $\ln([\text{B}]_0/[\text{B}]_t)$ gives the relative reaction rate coefficient. In these experiments A is $^{12}\text{CH}_4$ and B is $^{12}\text{CH}_3\text{D}$ or $^{13}\text{CH}_3\text{D}$.

100 2.2 Photoreactor

Experiments were carried out in the photochemical reactor at the University of Copenhagen, Department of Chemistry. The reactor has been described in detail elsewhere (Nilsson et al., 2009). It consists of a 100 L quartz cell with multi-pass optics surrounded by 16 UV-C fluorescent Hg lamps in a temperature controlled housing. The cell is coupled to a Bruker IFS 66v/S FTIR spectrometer
105 with either a mercury cadmium telluride (MCT) detector (Experiments 1–4) or an indium antimonide (InSb) (Experiments 5–16). The InSb-detector has a better signal-to-noise ratio, the MCT-detector is used in Experiments 1–4 for logistical reasons. Two thermocouple gauges are placed inside the temperature controlled housing to monitor the temperature and a pressure gauge is connected to the cell to monitor pressure inside the cell. The temperatures and the pressures were logged every 0.5 s.

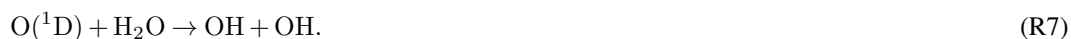
110 2.3 Laboratory procedure

Gas mixes were prepared by expanding H_2O vapor (Milli-Q Ultrapure Water) into the chamber through a glass gas manifold. The two methane isotopologues CH_3D (Experiments 1–8) (purity

> 98%, Cambridge Isotope Laboratories, Inc.) or $^{13}\text{CH}_3\text{D}$ (Experiments 9–16), and CH_4 (purity > 99%, Aldrich) and O_3 were flushed into the chamber with a N_2 buffer (purity 99.998%, Air Liquide), all at the concentrations given in Table 1. $^{13}\text{CH}_3\text{D}$ was synthesized using the Grignard reaction, see Joelsson et al. (2014). O_3 was generated from O_2 (purity 99.97 %, Air Liquide) using an ozone generator (Model AC-20, O_3 Technology), preconcentrated before injection on silica gel cooled with ethanol and dry ice to -67°C . The desired pressure in the cell (450 hPa) was obtained using N_2 as bath gas. The starting pressure is chosen such that the pressure is high enough for the N_2 to quench $\text{O}(^1\text{D})$ radicals, but low enough to keep the final pressure below atmospheric pressure. The gas mixture was left to rest for up to 1.5 hours while several IR spectra were recorded to ensure that no instability or dark chemistry occurs in the gas mix. The UV-C lamps were lit for up to 5 min photolyzing at least 75 % of the O_3 according to:



$\text{O}(^1\text{D})$ then subsequently reacts with H_2O to yield OH:



Up to 0.2 Pa O_3 was flushed with about 20 hPa N_2 into the chamber to compensate for the loss of ozone with time, mainly due to $\text{O}(^3\text{P}) + \text{O}_3$. A pressure gradient was established and maintained throughout the filling process such that no gas leaked back from the chamber into the gasline. Spectra were recorded at each filling step. The procedure was repeated until the mix had a final pressure of 933 hPa. Two experiments were conducted at each of the temperatures 278, 288, 298, and 313 K for each of the two heavy methane isotopologues. Exact temperatures are listed in Table 1. After each experiment a dilution test was performed: 133 hPa was pumped out and the chamber is refilled with 133 hPa N_2 . This was repeated 5–6 times. Ideally, concentration calculations from the spectral fits (data analysis described below) of the resulting spectra should give a linear fit with the slope of 1. The slope of these dilution tests are presented in Table 2. In an extra experiment with $^{12}\text{CH}_3\text{D}$, N_2O (Air Liquide, no purity information available) was added as an $\text{O}(^1\text{D})$ tracer. The results from this experiment are used as a benchmark to validate a model that was constructed to investigate the extent of $\text{O}(^1\text{D})$ chemistry, see Sect. 2.5. An example of an experimental plot can be found in Fig. 4 and the full data set in Figs. S1–S8 in the Supplement.

2.4 Data analysis

The experimental IR spectra were analyzed using the program MALT which simulates experimental FTIR spectra (Griffith, 1996) combined with non-linear least squares fitting to best-fit the calculated spectra to measured spectra (Griffith et al., 2012). The MALT program generates a simulated spectrum from initial estimates of the absorber concentrations and instrument parameters. The residual between the experimental and simulated spectra is reduced through iteration. Simulated line-shapes

Table 1. Experimental setup. The experiment numbers are listed in column Exp., the detector in the column Detect., the heavy CH₄ isotopologue included in the experiments are listed in column [^xCH₃D], the mean measured temperatures in the photoreactor are listed in column *T*, the H₂O-vapour concentrations at the start of the experiments (*t* = 0) as obtain from spectral fitting are listed in column [H₂O]_{*t*=0}, the mean O₃ concentration after refill (i.e. the “top”-values) as obtain from spectral fitting are listed in column [O₃]_{top}, the ¹²CH₄- concentrations at the start of the experiments (*t* = 0) as obtain from spectral fitting are listed in column [¹²CH₄]_{*t*=0}, and the heavy CH₄ concentrations at the start of the experiments (*t* = 0) as obtain from spectral fitting are listed in column [^xCH₃D]_{*t*=0}. Note that for the experiment including CH₃D, the value of initial concentration only refers to [¹²CH₃D]_{*t*=0}.

Exp.	Detect.	^x CH ₃ D	<i>T</i> /K	[H ₂ O] _{<i>t</i>=0} /hPa	[O ₃] _{top} /hPa	[¹² CH ₄] _{<i>t</i>=0} /hPa	[^x CH ₃ D] _{<i>t</i>=0} /hPa
1	MCT	CH ₃ D	298.2 ± 1.2	7.1	– ^a	0.030	0.054
2	MCT	CH ₃ D	297.6 ± 0.8	5.6	0.19	0.058	0.042
3	MCT	CH ₃ D	277.2 ± 0.2	5.2	0.29	0.109	0.046
4	MCT	CH ₃ D	277.0 ± 0.2	5.1	0.16	0.073	0.035
5	InSb	CH ₃ D	284.5 ± 0.1	7.2	0.26	0.025	0.033
6	InSb	CH ₃ D	291.1 ± 0.2	7.4	– ^a	0.052	0.050
7	InSb	CH ₃ D	313.5 ± 1.3	7.1	0.17	0.025	0.029
8	InSb	CH ₃ D	312.4 ± 0.9	4.3	– ^a	0.022	0.040
9	InSb	¹³ CH ₃ D	298.5 ± 0.1	5.1	– ^a	0.035	0.026
10	InSb	¹³ CH ₃ D	297.6 ± 0.6	6.4	0.13	0.025	0.033
11	InSb	¹³ CH ₃ D	276.8 ± 0.8	5.4	– ^a	0.024	0.024
12	InSb	¹³ CH ₃ D	277.2 ± 1.3	5.1	– ^a	0.022	0.030
13	InSb	¹³ CH ₃ D	287.4 ± 1.2	5.4	– ^a	0.021	0.028
14	InSb	¹³ CH ₃ D	287.4 ± 0.4	4.5	– ^a	0.016	0.029
15	InSb	¹³ CH ₃ D	314.4 ± 1.0	5.2	0.26	0.023	0.037
16	InSb	¹³ CH ₃ D	313.8 ± 0.8	8.3	0.17	0.025	0.035

^aSpectra recorded during or after photolysis, [O₃]_{top} not available

are generated using HITRAN absorption parameters (version 2008) (Rothman et al., 2009) con-
 volved with an FTIR instrument function simulating the Bruker IFS 66v/S instrument. The InSb
 detector covers a spectral range from 1800–5000 cm⁻¹ and the MCT detector covers a spectral
 150 range from 400–5000 cm⁻¹. The concentrations of ¹²CH₃D and ¹³CH₃D were calculated from
 spectral fits in the region 2140–2302 cm⁻¹, see Fig. 1 and 2. Interference from H₂O, CO₂, and CO
 was eliminated by including simulated spectra obtained from the HITRAN database in the fit. As
 there is no HITRAN data available for ¹³CH₃D in this region, the cross sections from 2000–2400
 cm⁻¹ for this isotopologue were estimated by shifting the spectrum of ¹²CH₃D, see Joëlsson et al.
 155 (2014). Concentrations of ¹²CH₄ were calculated from spectral fits in the region 2838–2997 cm⁻¹.

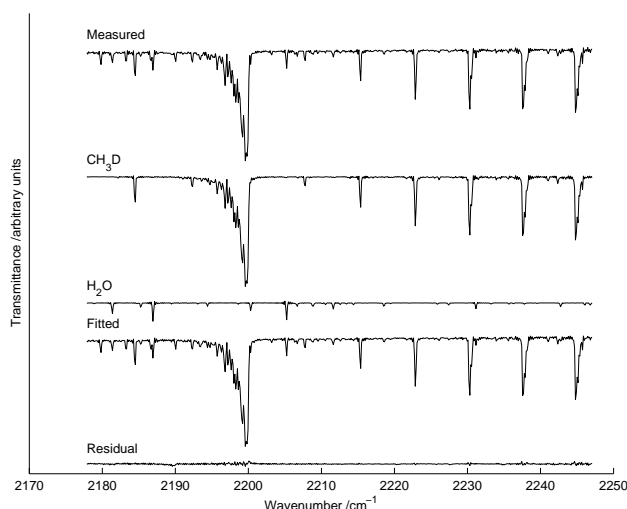


Figure 1. A typical spectral fit in the region where $[^{12}\text{CH}_3\text{D}]$ is obtained (Experiment 5). Experimental data are shown by the topmost line, followed by the fitted (synthetic) partial spectra of the most dominant absorbers (CH_3D and H_2O), the resulting fitted (synthetic) spectrum (also including CO_2 and CO), and the residual between the measured and fitted spectra is shown by the bottom line.

Interference from $^{13}\text{CH}_3\text{D}$ was reduced by including temperature adjusted reference spectra in the fit, and interference from $^{12}\text{CH}_3\text{D}$, H_2O , and H_2CO was by including simulated spectra obtained from the HITRAN database in the fit, see Fig. 3. The spectral windows were sometimes adjusted to exclude saturated lines.

160 After $[^x\text{CH}_3\text{D}]$ (where $x = 12$ or $x = 13$) and $[^{12}\text{CH}_4]$ were obtained from the spectral analysis, $\ln([^x\text{CH}_3\text{D}]_0/[^x\text{CH}_3\text{D}]_t)$ was plotted against $\ln([^{12}\text{CH}_4]_0/[^{12}\text{CH}_4]_t)$ as described in Sect. 2.1. A straight line was fitted to these data points using a weighted total least squares routine (York et al., 2004). The fitting procedure takes uncertainties in both dimensions into account. The uncertainty $\sigma(\ln([A]_0/[A]_t))$ was calculated using standard error propagation:

$$165 \quad \sigma(\ln([A]_0/[A]_t)) = \sqrt{\left(\frac{\sigma([A]_0)}{[A]_0}\right)^2 + \left(\frac{\sigma([A]_t)}{[A]_t}\right)^2} \quad (5)$$

where $\sigma([A])$ was obtained as output from MALT. The fitting procedure, performed using a MATLAB script (York et al., 2004), also yields an error estimation which is defined as the uncertainty of the kinetic isotope effect $\sigma(\alpha)$. An example of a straight line fit can be found in Fig. 4 and the full data set in Figs. S1–S8 in the Supplement. In the temperature dependence curve fitting procedure, 170 the parameters A and B are from a linearized version of the Arrhenius equation:

$$\ln(k) = \ln(A) + B \cdot T^{-1} \quad (6)$$

are adjusted to match experimental. Also here, the method of York et al. (2004) was used. The temperature in the cell was taken as the spatial average of the measurements from two thermocouples

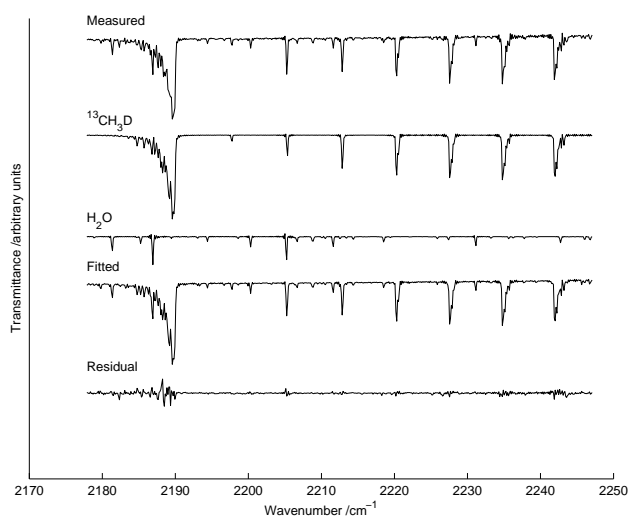


Figure 2. A typical spectral fit in the region where [$^{13}\text{CH}_3\text{D}$] is obtained (Experiment 10). Experimental data are shown by the topmost line, followed by the fitted (synthetic) partial spectra of the most dominant absorbers ($^{13}\text{CH}_3\text{D}$ and H_2O), the resulting fitted (synthetic) spectrum (also including CO_2 and CO), and the residual between the measured and fitted spectra is shown by the bottom line.

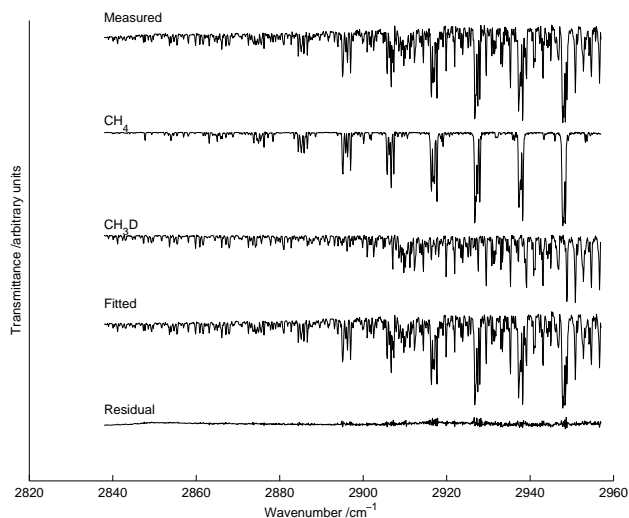


Figure 3. A typical spectral fit in the region where [$^{12}\text{CH}_4$] is obtained (Experiment 5). Experimental data are shown by the topmost line, followed by the fitted partial (synthetic) spectra of the most dominant absorbers (CH_4 and CH_3D), the resulting fitted (synthetic) spectrum (also including H_2O), and the residual between the measured and fitted spectra is shown by the bottom line.

inside the temperature housing. The experiment temperature was defined by the temporal mean
 175 of the spatially averaged temperature measurement series and the uncertainty of the experiment
 temperature was the standard deviation of the spatially averaged temperature measurement series.

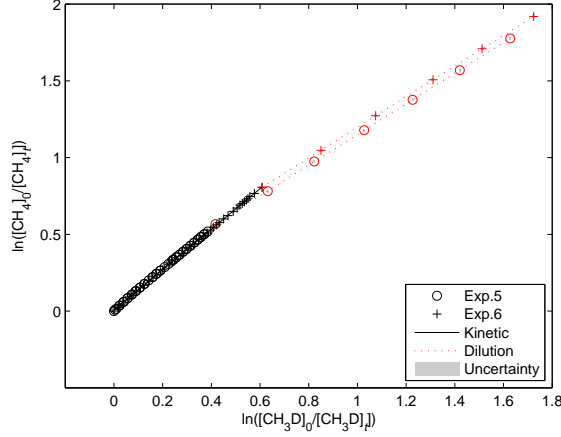


Figure 4. A typical experimental outcome, Experiment 5 and 6: CH₃D, $T = 288\text{K}$. Experimental data are shown using black open circles (Exp. 5) and black plus signs (Exp. 6). Corresponding dilution test points are shown using red symbols. A linear fit of the experimental points is shown using a black solid line and linear fit of the subsequent dilution test are represented by a red dotted line, uncertainties for each point are represented by gray areas.

2.5 Kinetic model

A kinetic model was used to determine the influence of $\text{O}(^1\text{D})$, reaction (R3), which rivals Reaction (R1). The model is previously described and was used by Nilsson et al. (2012). However, only the methane reaction subset and associated (O_x and HO_x) chemistry were used here. The Kintecus program (Ianni, 2003), simulates the photolysis of O_3 and the following oxidation chain of CH_4 . To model ozone photolysis accurately, the modeled O_3 was matched to the measured value by adjusting the photolysis rate, then the model was verified by comparing the decrease of CH_4 and the increase of H_2O during the experiment. The model was run for each refill of O_3 , where the reaction rates of Reactions (R1) and (R3) were obtained. The model was designed for room temperature; experiments at other temperatures were not modeled. Experiment 2 was thus modeled: 4.4% of CH_4 was estimated to be lost to Reaction (R3). In an additional experiment N_2O was introduced in the chamber as an $\text{O}(^1\text{D})$ -tracer. Since N_2O does not react with OH and is not photolyzed at the wavelengths present (Nilsson et al., 2009), the decreased of N_2O should be only due to Reaction (R8):



The amount of CH_4 lost by reaction (R3) can therefore be approximated by:

$$1 - \frac{[\text{CH}_4]_t}{[\text{CH}_4]_0} = 1 - \exp(-k_{(\text{R3})}[\text{O}(^1\text{D})]t) = 1 - \frac{[\text{N}_2\text{O}]_t}{[\text{N}_2\text{O}]_0}^{(k_{(\text{R8})}/k_{(\text{R3})})}, \quad (7)$$

where $k_{(R8)} = 1.27 \times 10^{-10} \text{cm}^{-3} \text{s}^{-1}$ and $k_{(R3)} = 1.75 \times 10^{-10} \text{cm}^{-3} \text{s}^{-1}$ (Sander et al., 2010). This gives 2.3% $[\text{CH}_4]$ lost by oxidation of $\text{O}(^1\text{D})$, Reaction (R3). The kinetic model described above estimated that 4.7 % $[\text{CH}_4]$ were lost by Reaction (R3) for this additional experiment. Both methods agree that $\text{O}(^1\text{D})$ loss is a minor channel. No correction is applied, and the possible deviation is included in the estimated error.

3 Theoretical procedure

Rate constants and kinetic isotope effects for $\text{CH}_4 + \text{OH}$ were calculated using a procedure similar to that employed by Joelsson et al. (2014).

3.1 Computational chemistry calculations

The geometries of reactants, products and transition states were determined using a geometry optimization procedure based on the unrestricted MP2 method (Møller and Plesset, 1934) and the aug-cc-pVQZ orbital basis set (Dunning Jr., 1989; Woon and Dunning Jr., 1993). Harmonic vibrational frequencies for all relevant isotopologues of reactants, products, and transition states were obtained at the same level of theory. The calculations were carried out using the Gaussian 09 program package (Frisch et al., 2009).

The electronic energy of the optimized structures were refined using the CCSD(T) method (Watts et al., 1993; Knowles et al., 1993, 2000) with aug-cc-pVTZ, aug-cc-pVQZ, and aug-cc-pV5Z basis sets. The results from the different basis sets were used to extrapolate the electronic energy at the complete basis set limit following the approach of Halkier et al. (1998) as described by Joelsson et al. (2014).

3.2 Rate constant calculations

The abstraction of a CH_4 hydrogen atom by OH can occur at four different sites. Depending on the methane isotopologue in question, these sites are either distinguishable or indistinguishable. Microscopic rate constants are calculated for hydrogen abstraction at each site using classical transition state theory with a tunneling correction factor,

$$k_{\text{micro}}^{(i)} = \eta_{\text{tun}}^{(i)} \frac{k_b T}{h} \frac{Q_{\text{TS}}^{(i)}}{Q_{\text{reac}}^{(i)}} \exp(-\Delta E^{(i)}/RT) \quad (8)$$

where $\Delta E^{(i)}$ is the reaction barrier height (including the zero point vibrational energy) for the i 'th reaction path. $\eta_{\text{tun}}^{(i)}$ is a tunneling correction factor obtained using the Wigner tunneling correction (Wigner, 1932). $Q_{\text{TS}}^{(i)}$ and $Q_{\text{reac}}^{(i)}$ are the partition functions for the transition state and reacting pair, respectively. The total rate constant is obtained by summing over the microscopic rate constants.

Table 2. Results. The experiment numbers are listed in column Exp., the heavy CH₄ isotopologue included in the experiments are listed in column ^xCH₃D, the mean measured temperatures in the photoreactor are listed in column *T*, the kinetic isotope effect corresponding to the isotopologue are listed in column α , and the result of the dilution experiments are listed in column k_{dil} .

Exp.	^x CH ₃ D	<i>T</i> /K	α	k_{dil}
1	CH ₃ D	298.2 ± 1.2	1.302 ± 0.038	1.011 ± 0.048
2	CH ₃ D	297.6 ± 0.8	1.314 ± 0.020	– ^a
3	CH ₃ D	277.2 ± 0.2	1.294 ± 0.017	0.962 ± 0.037
4	CH ₃ D	277.0 ± 0.2	1.335 ± 0.017	– ^a
5	CH ₃ D	284.5 ± 0.1	1.334 ± 0.012	0.999 ± 0.009
6	CH ₃ D	291.1 ± 0.2	1.323 ± 0.010	0.998 ± 0.010
7	CH ₃ D	313.5 ± 1.3	1.301 ± 0.007	1.006 ± 0.031
8	CH ₃ D	312.4 ± 0.9	1.338 ± 0.010	– ^a
9	¹³ CH ₃ D	298.5 ± 0.1	1.359 ± 0.022	1.000 ± 0.029
10	¹³ CH ₃ D	297.6 ± 0.6	1.314 ± 0.007	0.990 ± 0.064
11	¹³ CH ₃ D	276.8 ± 0.8	1.357 ± 0.046	1.016 ± 0.031
12	¹³ CH ₃ D	277.2 ± 1.3	1.344 ± 0.013	1.008 ± 0.030
13	¹³ CH ₃ D	287.4 ± 1.2	1.346 ± 0.025	1.009 ± 0.022
14	¹³ CH ₃ D	287.4 ± 0.4	1.342 ± 0.015	1.011 ± 0.019
15	¹³ CH ₃ D	314.4 ± 1.0	1.316 ± 0.016	1.003 ± 0.038
16	¹³ CH ₃ D	313.8 ± 0.8	1.331 ± 0.033	1.001 ± 0.034

^aNo dilution test performed

4 Results and Discussion

The results of the 16 individual experiments (eight for each isotopologue) are tabulated in Table 2. The resulting ^D α , ¹³C α , and ¹³C,^D α values from the experimental and theoretical studies are tabulated in Tables 3, 4, and 5 along with previous experimental and theoretical results. The results are also shown in Fig. 5 and 6 for reactions of CH₃D and ¹³CH₃D respectively.

The exponential curve fits yielded the parameters presented in Tables 3 and 5 giving ^D $\alpha_{\text{Arr}} = 1.32 \pm 0.13$ and ¹³C,^D $\alpha_{\text{Arr}} = 1.32 \pm 0.20$ at *T* = 298K. The mean of results of room temperature experiments Experiments 1 and 2, and Experiments 9 and 10 is ^D $\alpha_{\text{exp}} = 1.31 \pm 0.01$ and ¹³C,^D $\alpha_{\text{exp}} = 1.34 \pm 0.03$ respectively. It follows that $\gamma_{\text{exp}} = 1.02 \pm 0.02$ at *T* = 298K, using ¹³C $\alpha_{\text{exp}} = 1.0039 \pm 0.0002$ (Saueressig et al., 2001), meaning that the clumped isotope might react slower relative to what would be predicted based on the kinetic isotope effects of CH₃D and ¹³CH₄. However, if the Arrhenius parameters are used to calculate the kinetic isotope effects at *T* = 298K, $\gamma_{\text{Arr}} = 1.00 \pm 0.18$ (i.e. the reaction has no clumping effect). All uncertainties are given as one standard deviation (σ). The theoretical results gives $\gamma_{\text{theory}} = 1.00$ at *T* = 298K.

Table 3. Experimental and theoretical studies of ${}^D\alpha$. The temperature dependence studies are presented in the Arrhenius form ${}^D\alpha(T) = A(T/298\text{K})^n \exp(BT^{-1})$, where A , n , and B are tabulated, T is the given temperature range, and ${}^D\alpha(T = 298\text{K})$ is the resulting kinetic isotope effect at $T = 298\text{K}$. Where no B coefficient is presented A can be taken as ${}^D\alpha(T)$ for the given temperature range. All uncertainties are given as one standard deviation (σ).

Study	A	n	B/K	T/K	${}^D\alpha(T = 298\text{K})$
Experimental studies					
Present study ^a	1.23 ± 0.08	0	21 ± 21	[278,313]	1.31 ± 0.01^h
Saueressig et al. (2001) ^b	1.294 ± 0.009	–	–	296	–
Gierczak et al. (1997) ^c	1.09 ± 0.05	0	49 ± 11	[220,415]	1.25 ± 0.07
DeMore (1993) ^a	0.91	0	75	[298,360]	1.17
Gordon and Mulac (1975) ^d	1.50	–	–	416	–
Gordon and Mulac (1975) ^{d,i}	1.06	–	–	416	–
Theoretical studies					
Present study ^e	1.314	0	6.354	[200,300]	1.339
Sellevåg et al. (2006) ^f	[1.30, 1.00]	–	–	[200,1500]	1.27
Masgrau et al. (2001) ^{g,j}	1.00	-0.02	50.5	[200,1500]	1.25

^aFourier transform infrared spectroscopy - relative rate

^bTunable diode laser absorption spectroscopy - isotope ratio mass spectrometer

^cPulsed photolysis - pulsed laser-induced fluorescence

^dPulse radiolysis

^eTransition state theory with Wigner tunneling correction

^fCanonical unified statistical theory

^gMulticoefficient correlation method

^hAverage room temperature value, not obtained from curve fit

ⁱRe-evaluated by DeMore (1993)

^jArrhenius parameters available at (NIST, 2015)

The present experimental room temperature results for ${}^D\alpha$ agree, to within the error bars, with the previous experimental studies, with the exception of DeMore (1993). DeMore (1993) used FTIR spectroscopy with a slow flow setup where the two methane isotopologues were measured separately
240 with a common reference compound. The low ${}^D\alpha$ value in DeMore (1993) may be explained by interference from $\text{O}(^1\text{D})$ radicals: OH radicals were produced by photolysis of O_3 at 254 nm in the presence of H_2O , as in the present study. A relatively high rate of reaction (R3) would reduce the final kinetic isotope effect, since the kinetic isotope effect for oxidation with $\text{O}(^1\text{D})$ is smaller than the kinetic isotope effect for the oxidation of OH (Saueressig et al., 2001). The present experimental
245 results of ${}^D\alpha$ are also in good agreement with Masgrau et al. (2001) and Sellevåg et al. (2006). The theoretical calculations of ${}^D\alpha$ give a slightly higher value than the experimental results, although they are in good agreement with the best Arrhenius curve fit at $T = 298\text{K}$.

Table 4. Experimental and theoretical studies of $^{13}\text{C}\alpha$. The temperature dependence studies are presented in the Arrhenius form $^{13}\text{C}\alpha(T) = A \exp(BT^{-1})$, where A and B are tabulated, T is the given temperature range, and $^{13}\text{C}\alpha(T = 298\text{K})$ is the resulting kinetic isotope effect at $T = 298\text{K}$. Where no B coefficient is presented A can be taken as $^{13}\text{C}\alpha(T)$ for the given temperature range. All uncertainties are given as one standard deviation (σ).

Study	A	B/K	T/K	$^{13}\text{C}\alpha(T = 298\text{K})$
Experimental studies				
Saueressig et al. (2001) ^a	1.0039 ± 0.0002	–	296	–
Cantrell et al. (1990) ^b	1.0054 ± 0.0005	–	[273, 353]	1.0054 ± 0.0005
Rust and Stevens (1980) ^{c,i}	1.003	–	–	–
Theoretical studies				
Present study ^d	1.0137	-1.219	[200,300]	1.0094
Sellevåg et al. (2006) ^e	[1.014, 1.00]	–	[200,1500]	1.003
Gupta et al. (1997) ^f	1.010	–	300	–
Melissas and Truhlar (1993) ^{g,h}	[1.005, 1.001]	–	[223,416]	1.005
Lasaga and Gibbs (1991) ^h	[1.0036, 1.0076]	–	[150,350]	–

^aTunable diode laser absorption spectroscopy - isotope ratio mass spectrometer

^bGas chromatography - mass spectrometry

^cIsotope ratio mass spectrometry

^dTransition state theory with Wigner tunneling correction

^eCanonical variational transition state theory

^fConventional transition state theory

^gInterpolated variational transition state theory with centrifugal-dominant, small-curvature tunneling coefficients

^hAb initio calculations

ⁱNo temperature information available

Table 5. Experimental and theoretical studies of $^{13}\text{C,D}\alpha$. The temperature dependencies are presented in the Arrhenius form $^{13}\text{C,D}\alpha(T) = A \exp(BT^{-1})$, where A and B are tabulated, T is the given temperature range, and $^{13}\text{C,D}\alpha(T = 298\text{K})$ is the resulting kinetic isotope effect at $T = 298\text{K}$. All uncertainties are given as one standard deviation (σ).

Study	A	B/K	T/K	$^{13}\text{C,D}\alpha(T = 298\text{K})$
Experimental study ^a	1.18 ± 0.10	38 ± 26	[278,313]	1.34 ± 0.03^c
Theoretical study ^b	1.328	5.301	[200,300]	1.349

^aFourier transform infrared spectroscopy - relative rate

^bTransition state theory with Wigner tunneling correction

^cAverage room temperature value, not obtained from curve fit

The experimental room temperature result for $^{13}\text{C,D}\alpha = 1.34 \pm 0.03$ agrees to within the error bar with both the theoretical value and the best estimate of the Arrhenius curve fit at $T = 298\text{K}$.

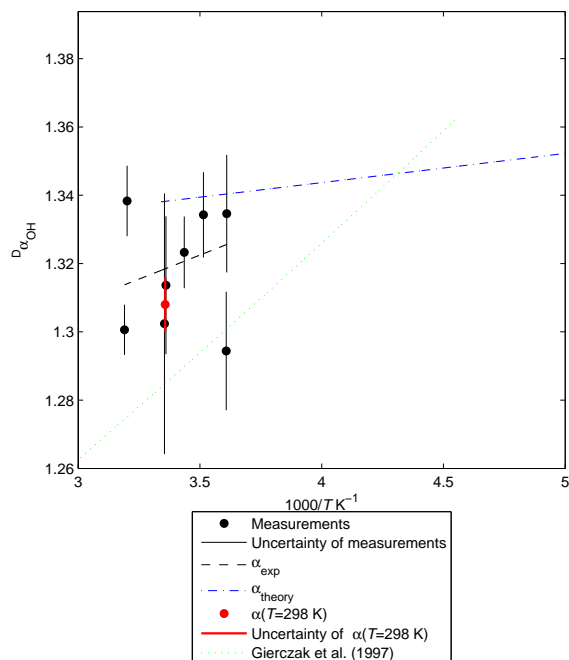


Figure 5. The individual measurements of $^D\alpha$, are represented by black points; the accompanying individual error bars are represented by thin black solid lines; the experimental Arrhenius curve fit is represented by a black dashed line; the theoretical Arrhenius curve fit is represented by a blue dashed-dotted line; the mean of the room temperature measurements are represented by a red solid circle; the uncertainty of the room temperature measurements are represented by a thick red solid line; the result from Gierczak et al. (1997) (which is included for comparison) are represented by a green dotted line. All uncertainties are given as one standard deviation (σ).

250 The theoretical calculations show a very small temperature dependence; the variability in the experimental data is large compared to the value of the slope, making a quantification of the temperature dependence uncertain. Furthermore, the theoretical analysis revealed that the primary cause for the kinetic isotope effect is the substantially reduced reactivity of the D atom, which, in turn, can be explained by a significant increase in reaction barrier due to changes in vibrational zero point energy
255 and to a lesser extent tunneling.

4.1 Atmospheric implications

At steady state, assuming no clumping in emissions, $\Delta(^{13}\text{CH}_3\text{D}) = \ln(\gamma)$. It follows that $\Delta(^{13}\text{CH}_3\text{D}) = 0.02 \pm 0.02$ implying that the clumped isotope effect of the OH reaction is small. Wang et al. (2015) have studied a variety of natural samples and found $\Delta(^{13}\text{CH}_3\text{D})$ values that vary from

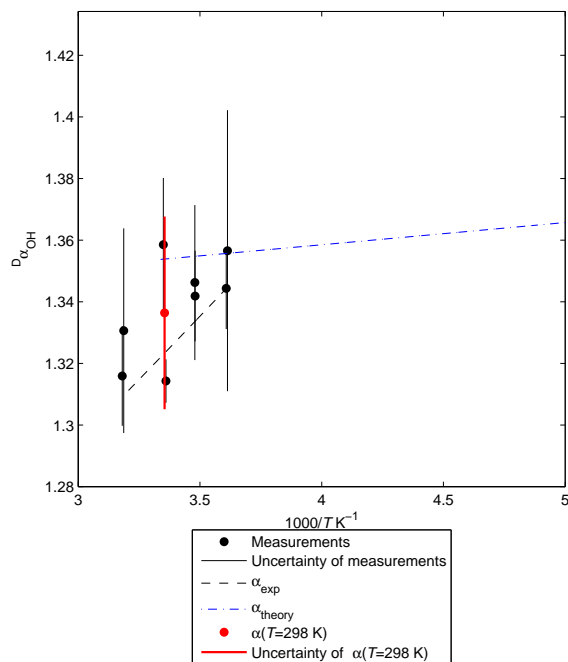


Figure 6. The individual measurements of $^{13}\text{C},\text{D}\alpha$, are represented by black points; the accompanying individual error bars are represented by thin black solid lines; the experimental Arrhenius curve fit is represented by a black dashed line; the theoretical Arrhenius curve fit is represented by a blue dashed-dotted line; the mean of the room temperature measurements are represented by a red solid circle; the uncertainty of the room temperature measurements are represented by a thick red solid line. All uncertainties are given as one standard deviation (σ).

260 $(-3.36 \pm 1.42)\text{‰}$ for samples of bubbling gases from The Cedars, Cazadero, California, USA, to
 $(6.17 \pm 0.34)\text{‰}$ for samples from gas voids and hydrates in sediment cores from the Northern Cas-
 cadia Margin. Methanogenic bacteria in the laboratory ranged from -1.34‰ to 2.29‰ . Natural gas
 was found to vary from 2.53‰ to 5.18‰ . Given these natural variations in $\Delta(^{13}\text{CH}_3\text{D})$ values of the
 sources, it is clear from isotopic mass balance that the fractionation from atmospheric oxidation by
 265 OH will likely have little effect on the observed $\Delta(^{13}\text{CH}_3\text{D})$ value of tropospheric methane. Rather,
 this number will reflect the relative contributions of the sources. $\Delta(^{13}\text{CH}_3\text{D})$ would therefore be a
 more straightforward tracer for tracking methane sources than conventional isotopic analysis. Fur-
 further field studies are clearly needed to characterize $\Delta(^{13}\text{CH}_3\text{D})$ values of microbial and thermal
 methane.

270 5 Conclusions

We present experimentally derived $\text{CH}_4 + \text{OH}$ kinetic isotope effects and their temperature dependence for CH_3D and $^{13}\text{CH}_3\text{D}$; the latter is reported for the first time. We find $^{\text{D}}\alpha = 1.31 \pm 0.01$ and $^{13\text{C,D}}\alpha = 1.34 \pm 0.03$ at room temperature, implying that the kinetic isotope effect is multiplicative such that $(k_{\text{CH}_4}/k_{^{13}\text{CH}_4})(k_{\text{CH}_4}/k_{\text{CH}_3\text{D}}) = k_{\text{CH}_4}/k_{^{13}\text{CH}_3\text{D}}$ to within the experimental uncertainty.

275 We compare our experimental results to theoretical estimates derived using transition state theory with tunneling correction and kinetic isotope effects reported in the literature. We find good agreement between theoretical and literature values. Based on these experiments we find that the OH reaction (the main sink of methane) at steady-state has a clumped $\Delta(^{13}\text{CH}_3\text{D}) = 0.02 \pm 0.02$.

Acknowledgements. This research has received funding from the European Community's Seventh Framework Programme (FP7/2007-2013) under grant agreement No. 237890, the Carlsberg foundation, and the Danish Council for Independent Research.

References

- Allan, W., Lowe, D., and Cainey, J.: Active chlorine in the remote marine boundary layer: Modeling anomalous measurements of $\delta^{13}\text{C}$ in methane, *Geophysical research letters*, 28, 3239–3242, 2001a.
- 285 Allan, W., Manning, M., Lassey, K., Lowe, D., and Gomez, A.: Modeling the variation of $\delta^{13}\text{C}$ in atmospheric methane: Phase ellipses and the kinetic isotope effect, *Global biogeochemical cycles*, 15, 467–481, 2001b.
- Bergamaschi, P., Bräunlich, M., Marik, T., and Brenninkmeijer, C. A.: Measurements of the carbon and hydrogen isotopes of atmospheric methane at Izaña, Tenerife: Seasonal cycles and synoptic-scale variations, *Journal of Geophysical Research: Atmospheres*, 105, 14 531–14 546, 2000.
- 290 Cantrell, C., Shetter, R., Mcdaniel, A., Calvert, J., Davidson, J., Lowe, D., Tyler, S., Cicerone, R., and Greenberg, J.: Carbon Kinetic Isotope Effect in the Oxidation of Methane by the Hydroxyl Radical, *J. Geophys. Res.*, 95, 22 455–22 462, 1990.
- Ciais, P., Sabine, C., Bala, G., Bopp, L., Brovkin, V., Canadell, J., Chhabra, A., DeFries, R., Galloway, J., Heimann, M., Jones, C., Le Quéré, C., Myneni, R., Piao, S., and Thornton, P.: Carbon and Other Biogeochemical Cycles. In: *Climate Change 2013: The Physical Science Basis. Contribution of Working Group I to the Fifth Assessment Report of the Intergovernmental Panel on Climate Change*, Cambridge University Press, Cambridge, United Kingdom and New York, NY, USA, 2013.
- 295 Crowley, J. N., Saueressig, G., Bergamaschi, P., Fischer, H., and Harris, G. W.: Carbon kinetic isotope effect in the reaction $\text{CH}_4 + \text{Cl}$: a relative rate study using FTIR spectroscopy, *Chem. Phys. Lett.*, 303, 268–274, 1999.
- 300 DeMore, W.: Rate constant ratio for the reactions of OH with CH_3D and CH_4 , *Journal of physical chemistry*, 97, 8564–8566, 1993.
- Dunning Jr., T. H.: Gaussian basis sets for use in correlated molecular calculations. I. The atoms boron through neon and hydrogen, *J. Chem. Phys.*, 90, 1007–1023, 1989.
- 305 Eiler, J. M., Clog, M., Magyar, P., Piasecki, A., Sessions, A., Stolper, D., Deerberg, M., Schlueter, H. J., and Schwieters, J.: A high-resolution gas-source isotope ratio mass spectrometer, *International Journal of Mass Spectrometry*, 335, 45–56, 2013.
- Feilberg, K. L., Griffith, D. W. T., Johnson, M. S., and Nielsen, C. J.: The ^{13}C and D kinetic isotope effects in the reaction of CH_4 with Cl, *Int. J. Chem. Kinet.*, 37, 110–118, 2005.
- 310 Ferretti, D. F., Miller, J. B., White, J. W. C., Etheridge, D. M., Lassey, K. R., Lowe, D. C., Meure, C. M. M., Dreier, M. F., Trudinger, C. M., van Ommen, T. D., and Langenfelds, R. L.: Unexpected changes to the global methane budget over the past 2000 years, *Science*, 309, 1714–1717, 2005.
- Frisch, M. J., Trucks, G. W., Schlegel, H. B., Scuseria, G. E., Robb, M. A., Cheeseman, J. R., Scalmani, G., Barone, V., Mennucci, B., Petersson, G. A., Nakatsuji, H., Caricato, M., Li, X., Hratchian, H. P., Izmaylov, 315 A. F., Bloino, J., Zheng, G., Sonnenberg, J. L., Hada, M., Ehara, M., Toyota, K., Fukuda, R., Hasegawa, J., Ishida, M., Nakajima, T., Honda, Y., Kitao, O., Nakai, H., Vreven, T., Montgomery, Jr., J. A., Peralta, J. E., Ogliaro, F., Bearpark, M., Heyd, J. J., Brothers, E., Kudin, K. N., Staroverov, V. N., Kobayashi, R., Normand, J., Raghavachari, K., Rendell, A., Burant, J. C., Iyengar, S. S., Tomasi, J., Cossi, M., Rega, N., Millam, J. M., Klene, M., Knox, J. E., Cross, J. B., Bakken, V., Adamo, C., Jaramillo, J., Gomperts, R., 320 Stratmann, R. E., Yazyev, O., Austin, A. J., Cammi, R., Pomelli, C., Ochterski, J. W., Martin, R. L., Morokuma, K., Zakrzewski, V. G., Voth, G. A., Salvador, P., Dannenberg, J. J., Dapprich, S., Daniels, A. D.,

- Farkas, O., Foresman, J. B., Ortiz, J. V., Cioslowski, J., and Fox, D. J.: Gaussian 09 Revision A.1, gaussian Inc. Wallingford CT 2009, 2009.
- 325 Gierczak, T., Talukdar, R. K., Herndon, S. C., Vaghjiani, G. L., and Ravishankara, A. R.: Rate Coefficients
for the Reactions of Hydroxyl Radicals with Methane and Deuterated Methanes, *J. Phys. Chem. A*, 101,
3125–3134, 1997.
- Gordon, S. and Mulac, W. A.: Reaction of OH(X²-PI) radical produced by pulse-radiolysis of water-vapor,
International Journal of Chemical Kinetics, 1, 289–299, 1975.
- 330 Griffith, D., Deutscher, N., Caldow, C., Kettlewell, G., Riggensbach, M., and Hammer, S.: A Fourier transform
infrared trace gas analyser for atmospheric applications, *Atmospheric Measurement Techniques Discussions*,
5, 3717–3769, 2012.
- Griffith, D. W. T.: Synthetic Calibration and Quantitative Analysis of Gas-Phase FT-IR Spectra, *Appl. Spec-*
trosc., 50, 59–70, 1996.
- Gupta, M. L., McGrath, M. P., Cicerone, R. J., Rowland, F. S., and Wolfsberg, M.: C-12/C-13 kinetic isotope
335 effects in the reactions of CH₄ with OH and Cl, *Geophysical Research Letters*, 24, 2761–2764, 1997.
- Halkier, A., T., H., Jørgensen, P., Klopper, W., Koch, H., Olsen, J., and Wilson, A. K.: Basis-set convergence in
correlated calculations on Ne, N₂, and H₂O, *Chem. Phys. Lett.*, 286, 243 – 252, 1998.
- Ianni, J.: A Comparison of the Bader-Deuflhard and the Cash-Karp Runge-Kutta Integrators for the GRI-MECH
3.0 Model Base on the Chemical Kinetics Code Kintecus, 2003.
- 340 IPCC: Climate Change 2013: The Physical Science Basis. Contribution of Working Group I to the Fifth Assess-
ment Report of the Intergovernmental Panel on Climate Change, Cambridge University Press, Cambridge,
United Kingdom and New York, NY, USA, 2013.
- Joelsson, L. M. T., Forecast, R., Schmidt, J. A., Meusinger, C., Nilsson, E. J. K., Ono, S., and Johnson, M. S.:
Relative rate study of the kinetic isotope effect in the (CH₃D)-C-13 + Cl reaction, *Chemical Physics Letters*,
345 605, 152–157, 2014.
- Kirschke, S., Bousquet, P., Ciais, P., Saunois, M., Canadell, J. G., Dlugokencky, E. J., Bergamaschi, P.,
Bergmann, D., Blake, D. R., Bruhwiler, L., et al.: Three decades of global methane sources and sinks, *Nature*
Geoscience, 6, 813–823, 2013.
- Knowles, P. J., Hampel, C., and Werner, H.-J.: Coupled cluster theory for high spin, open shell reference wave
350 functions, *J. Chem. Phys.*, 99, 5219–5227, 1993.
- Knowles, P. J., Hampel, C., and Werner, H.-J.: Erratum: “Coupled cluster theory for high spin, open shell
reference wave functions” [*J. Chem. Phys.* 99, 5219 (1993)], *J. Chem. Phys.*, 112, 3106–3107, 2000.
- Lasaga, A. C. and Gibbs, G.: Ab initio studies of the kinetic isotope effect of the CH₄ + OH• atmospheric
reaction, *Geophysical Research Letters*, 18, 1217–1220, 1991.
- 355 Lassey, K. R., Etheridge, D. M., Lowe, D. C., Smith, A. M., and Ferretti, D. F.: Centennial evolution of the
atmospheric methane budget: what do the carbon isotopes tell us?, *Atmos. Chem. and Phys.*, 7, 2119–2139,
2007.
- Liu, Q. and Liu, Y.: Clumped-isotope signatures at equilibrium of CH₄, NH₃, H₂O, H₂S and SO₂,
Geochimica et Cosmochimica Acta, 175, 252–270, 2016.

- 360 Lowe, D. C., Manning, M. R., Brailsford, G. W., and Bromley, A. M.: The 1991-1992 atmospheric methane anomaly: Southern Hemisphere C-13 decrease and growth rate fluctuations, *Geophys. Res. Lett.*, 24, 857–860, 1997.
- Ma, Q., Wu, S., and Tang, Y.: Formation and abundance of doubly-substituted methane isotopologues ((CH₃D)-C-13) in natural gas systems, *Geochim. Cosmochim. Acta*, 72, 5446–5456, 2008.
- 365 Masgrau, L., Gonzalez-Lafont, A., and Lluch, J. M.: The reactions CH_nD_{4-n} + OH → P and CH₄ + OD → CH₃ + HOD as a test of current direct dynamics multicoefficient methods to determine variational transition state rate constants. II, *Journal of Chemical Physics*, 115, 4515–4526, 2001.
- Melissas, V. S. and Truhlar, D. G.: Deuterium and C-13 kinetic isotope effects for the reaction of OH with CH₄, *Journal of Chemical Physics*, 99, 3542–3552, 1993.
- 370 Møller, C. and Plesset, M. S.: Note on an Approximation Treatment for Many-Electron Systems, *Phys. Rev.*, 46, 618–622, 1934.
- Nilsson, E. J. K., Eskebjerg, C., and Johnson, M. S.: A photochemical reactor for studies of atmospheric chemistry, *Atmospheric Environment*, 43, 3029–3033, 2009.
- Nilsson, E. J. K., Andersen, V. F., Nielsen, O. J., and Johnson, M. S.: Rate coefficients for the chemical reactions of CH₂F₂, CHClF₂, CH₂FCF₃ and CH₃CCl₃ with O(¹D) at 298 K, *Chemical Physics Letters*, 554, 27–32, 2012.
- 375 NIST: National Institute of Standards and Technology Chemical Kinetics Database, <http://kinetics.nist.gov>, last access: 2 October 2015, 2015.
- Ono, S., Wang, D. T., Gruen, D. S., Sherwood Lollar, B., Zahniser, M. S., McManus, B. J., and Nelson, D. D.: Measurement of a Doubly Substituted Methane Isotopologue, ¹³CH₃D, by Tunable Infrared Laser Direct Absorption Spectroscopy, *Analytical chemistry*, 86, 6487–6494, 2014.
- 380 Pohlman, J., Kaneko, M., Heuer, V., Coffin, R., and Whiticar, M.: Methane sources and production in the northern Cascadia margin gas hydrate system, *Earth and Planetary Science Letters*, 287, 504–512, 2009.
- Quay, P., Stutsman, J., Wilbur, D., Snover, A., Dlugokencky, E., and Brown, T.: The isotopic composition of atmospheric methane, *Global Biogeochemical Cycles*, 13, 445–461, 1999.
- 385 Rothman, L. S., Gordon, I. E., Barbe, A., Benner, Bernath, P. F., Birk, M., Boudon, V., Brown, L. R., Campargue, A., and Champion, J. P.: The HITRAN 2008 molecular spectroscopic database, *J. Quant. Spec. and Rad. Trans.*, 110, 533–572, 2009.
- Rust, F. and Stevens, C.: Carbon kinetic isotope effect in the oxidation of methane by hydroxyl, *International Journal of Chemical Kinetics*, 12, 371–377, 1980.
- 390 Sander, S. P., Friedl, R., Barker, J., Golden, D., Kurylo, M., Moortgat, G., Wine, P., Abbatt, J., Burkholder, J., Kolb, C., Moortgat, G., Huie, R., VL, O., et al.: Chemical kinetics and photochemical data for use in atmospheric studies: evaluation number 17, National Aeronautics and Space Administration, Jet Propulsion Laboratory, California Institute of Technology Pasadena, CA, 2010.
- 395 Saueressig, G., Bergamaschi, P., Crowley, J. N., Fischer, H., and Harris, G. W.: Carbon kinetic isotope effect in the reaction of CH₄ with Cl atoms, *Geophys. Res. Lett.*, 22, 1225–1228, 1995.
- Saueressig, G., Bergamaschi, P., Crowley, J. N., Fischer, H., and Harris, G. W.: D/H kinetic isotope effect in the reaction CH₄ + Cl, *Geophys. Res. Lett.*, 23, 3619–3622, 1996.

- Saueressig, G., Crowley, J. N., Bergamaschi, P., Bruhl, C., Brenninkmeijer, C. A. M., and Fischer, H.: Carbon
400 ¹³ and D kinetic isotope effects in the reactions of CH₄ with O(D-1) and OH: New laboratory measurements
and their implications for the isotopic composition of stratospheric methane, *J. Geophys. Res.-Atmos.*, 106,
23 127–23 138, 2001.
- Schmidt, J. A. and Johnson, M. S.: Clumped isotope perturbation in tropospheric nitrous oxide from strato-
spheric photolysis, *Geophysical Research Letters*, 42, 3546–3552, 2015.
- 405 Schmidt, J. A., Johnson, M. S., and Schinke, R.: Carbon dioxide photolysis from 150 to 210 nm: Singlet and
triplet channel dynamics, UV-spectrum, and isotope effects, *Proceedings of the National Academy of Sci-
ences*, 110, 17 691–17 696, 2013.
- Sellevåg, S. R., Nyman, G., and Nielsen, C. J.: Study of the carbon-13 and deuterium kinetic isotope effects in
the Cl and OH reactions of CH₄ and CH₃Cl, *Journal of Physical Chemistry A*, 110, 141–152, 2006.
- 410 Stolper, D. A., Sessions, A. L., Ferreira, A. A., Santos Neto, E. V., Schimmelmann, A., Shusta, S. S., Valentine,
D. L., and Eiler, J. M.: Combined C-13-D and D-D clumping in methane: Methods and preliminary results,
Geochimica Et Cosmochimica Acta, 126, 169–191, 2014.
- Tyler, S. C., Rice, A. L., and Ajje, H. O.: Stable isotope ratios in atmospheric CH₄: Implications for seasonal
sources and sinks, *J. Geophys. Res.-Atmos.*, 112, 2007.
- 415 Wang, D. T., Gruen, D. S., Lollar, B. S., Hinrichs, K.-U., Stewart, L. C., Holden, J. F., Hristov, A. N., Pohlman,
J. W., Morrill, P. L., Koenneke, M., Delwiche, K. B., Reeves, E. P., Sutcliffe, C. N., Ritter, D. J., Seewald,
J. S., McIntosh, J. C., Hemond, H. F., Kubo, M. D., Cardace, D., Hoehler, T. M., and Ono, S.: Nonequilibrium
clumped isotope signals in microbial methane, *Science*, 348, 428–431, 2015.
- Watts, J. D., Gauss, J., and Bartlett, R. J.: Coupled-cluster methods with noniterative triple excitations for
420 restricted open-shell Hartree–Fock and other general single determinant reference functions. Energies and
analytical gradients, *J. Chem. Phys.*, 98, 8718–8733, 1993.
- Wigner, E.: On the quantum correction for thermodynamic equilibrium, *Physical Review*, 40, 749, 1932.
- Woon, D. E. and Dunning Jr., T. H.: Gaussian basis sets for use in correlated molecular calculations. III. The
atoms aluminum through argon, *J. Chem. Phys.*, 98, 1358–1371, 1993.
- 425 York, D., Evensen, N. M., Martínez, M. L., and De Basable Delgado, J.: Unified equations for the slope, inter-
cept, and standard errors of best straight line, *Am. J. Phys.*, 72, 367–375, 2004.